Title
Incipient microphase separation in short chain perfluoropolyether- block -poly(ethylene oxide) copolymers

Journal
Soft Matter, 13(22)

ISSN
1744-683X

Authors
Chintapalli, Mahati
Timachova, Ksenia
Olson, Kevin R
et al.

Publication Date
2017-06-07

DOI
10.1039/c7sm00738h

Peer reviewed

Soft Matter

PAPER

View Article Online
View Journal | View Issue

Cite this: Soft Matter, 2017, 13, 4047

Incipient microphase separation in short chain perfluoropolyether-*block*-poly(ethylene oxide) copolymers†

Mahati Chintapalli,[ab] Ksenia Timachova,[bc] Kevin R. Olson,[d] Michał Banaszak,[e] Jacob L. Thelen,[bc] Sue J. Mecham,[d] Joseph M. DeSimone[dg] and Nitash P. Balsara*[bcf]

Received 13th April 2017,
Accepted 9th May 2017

DOI: 10.1039/c7sm00738h

rsc.li/soft-matter-journal

Incipient microphase separation is observed by wide angle X-ray scattering (WAXS) in short chain multiblock copolymers consisting of perfluoropolyether (PFPE) and poly(ethylene oxide) (PEO) segments. Two PFPE–PEO block copolymers were studied; one with dihydroxyl end groups and one with dimethyl carbonate end groups. Despite having a low degree of polymerization ($N \sim 10$), these materials exhibited significant scattering intensity, due to disordered concentration fluctuations between their PFPE-rich and PEO-rich domains. The disordered scattering intensity was fit to a model based on a multicomponent random phase approximation to determine the value of the interaction parameter, χ, and the radius of gyration, R_g. Over the temperature range 30–90 °C, the values of χ were determined to be very large ($\sim$2–2.5), indicating a high degree of immiscibility between the PFPE and PEO blocks. In PFPE–PEO, due to the large electron density contrast between the fluorinated and non-fluorinated block and the high value of χ, disordered scattering was detected at intermediate scattering angles, ($q \sim 2$ nm^{-1}) for relatively small polymer chains. Our ability to detect concentration fluctuations was enabled by both a relatively large value of χ and significant scattering contrast.

Introduction

Perfluoropolyethers (PFPE) are a class of short chain polymers that are traditionally used as lubricants.[1–3] More recent applications of these materials include antifouling surface coatings, lithium battery electrolytes, and surfactants.[4–10] In this paper, we study the thermodynamic properties of the four PFPEs described in Table 1. The two versions of diol-terminated PFPEs are commercially available: $PFPE_{D10}$–Diol and $PFPE_{E10}$–Diol (see Table 1 for structures). $PFPE_{D10}$–Diol is a random copolymer of CF_2CF_2O and CF_2O groups with diol end groups. $PFPE_{E10}$–Diol is a short ABA triblock copolymer with two short poly(ethylene oxide) (PEO) chains attached to the ends of the fluorinated random copolymer. In a previous publication, we demonstrated that simple chemical reactions may be used to convert diol end groups into dimethyl carbonate (DMC) end groups to give $PFPE_{D10}$–DMC and $PFPE_{E10}$–DMC.[8]

The purpose of this paper is to characterize the four PFPEs given in Table 1. When viewed by the naked eye, all of these compounds appear to be simple homogeneous liquids. However, hydrocarbons such as PEO have very limited miscibility with fluorinated compounds. The formation of small PEO-rich microphases in $PFPE_{E10}$–Diol and $PFPE_{E10}$–DMC is therefore possible. Our objective is to examine this possibility in $PFPE_{E10}$–Diol and $PFPE_{E10}$–DMC; the $PFPE_{D10}$–Diol and $PFPE_{D10}$–DMC samples mainly provide the baseline for our analysis. Whether or not two-component block copolymers undergo microphase separation depends on the linear arrangements of the segments, the volume fraction of one of the components ϕ, the average number of statistical segments per chain, N, and the Flory–Huggins interaction parameter χ.[11–13]

In disordered ABA triblock copolymers, concentration fluctuations between the A and B segments occur at a characteristic length scale, which can be detected by X-ray or neutron

[a] Department of Materials Science and Engineering, University of California, Berkeley, California 94720, USA
[b] Materials Sciences Division, Lawrence Berkeley National Laboratory, Berkeley, California 94720, USA. E-mail: nbalsara@berkeley.edu
[c] Department of Chemical and Biomolecular Engineering, University of California, Berkeley, California 94720, USA
[d] Department of Chemistry, University of North Carolina at Chapel Hill, Chapel Hill, North Carolina 27599, USA
[e] Faculty of Physics and NanoBioMedical Centre, A. Mickiewicz University, ul. Umultowska 85, 61 614 Poznan, Poland
[f] Environmental Energy Technologies Division, Lawrence Berkeley National Laboratory, Berkeley, California 94720, USA
[g] Department of Chemical and Biomolecular Engineering, North Carolina State University, Raleigh, North Carolina, 27695, USA

† Electronic supplementary information (ESI) available. See DOI: 10.1039/c7sm00738h

Table 1 Structure of polymers used in this study. The average numbers of the tetrafluoroethylene oxide groups, m, the difluoromethylene oxide groups, n, and the ethylene oxide groups, q are given. The number of ethylene oxide groups per chain is $2q$

Polymer	Structure of uncoupled component	m	n	q
$PFPE_{D10}$–Diol	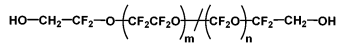	7	3	0
$PFPE_{D10}$–DMC	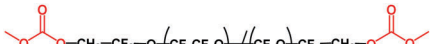	7	3	0
$PFPE_{E10}$–Diol	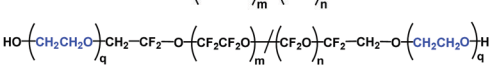	5	4	2
$PFPE_{E10}$–DMC	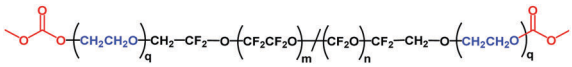	5	4	2

scattering experiments.[14,15] These concentration fluctuations are described using the random phase approximation (RPA) theory developed by Leibler and later expanded on by Fredrickson and Helfand.[13,16] Typically, the scattering that occurs due to concentration fluctuations is observed at small angles, where the scattering vector, $q = \frac{4\pi \sin\theta}{\lambda}$, is below approximately 1 nm^{-1} (corresponding to fluctuation length scales above ~5 nm). Here, θ is the scattering angle, and λ is the wavelength of the radiation. In contrast to previous studies of disordered concentration fluctuations that have used either SAXS or SANS,[14,15,17–19] we use wide angle X-ray scattering (WAXS) due to the short chain lengths of the materials studied. Given the relatively large scattering angles, angle-dependent scattering corrections are developed to reduce the scattering data. In the traditional RPA model, the polymers are assumed to be monodisperse.[13] $PFPE_{E10}$–Diol is a commercial sample that is known to contain the products of chain coupling reactions. The volume fractions of the uncoupled ABA triblock copolymer, the dimerized ABABA pentablock copolymer, the trimerized ABABABA heptablock copolymer, and the tetramerized ABABABABA nonablock copolymer are given by φ_1–φ_4, respectively. The reaction to produce the $PFPE_{E10}$–DMC polymer from the $PFPE_{E10}$–Diol precursor has been shown to increase chain coupling.[20] $PFPE_{E10}$–Diol comprises 12% of coupled products, while $PFPE_{E10}$–DMC comprises 57% of coupled products, as shown in Table 2. Our RPA analysis accounts for the presence of coupled products.

In Table 2, the data from ref. 20 are reported: the number-averaged molecular weight of the mixture, $M_{n,Ave}$, the dispersity of the mixture, $Đ_{Ave}$, the number-averaged molecular weight of the uncoupled component, $M_{n,1}$, and the dispersity of the uncoupled component, $Đ_1$.[20] In this study, using WAXS measurements and a modified multiblock RPA model, we report on the structure and interaction strength in short chain PFPE–PEO block copolymers.

Table 2 Composition and molecular weight of polymers in this study. The volume fractions of each component, the uncoupled, monomeric ABA triblock chain, dimer, trimer and tetramer are given by φ_1, φ_2, φ_3, and φ_4. The number average molecular weight and dispersity are given for both the mixtures of coupled components, $M_{n,Ave}$ and $Đ_{Ave}$, and the simple, uncoupled ABA triblock, $M_{n,1}$ and $Đ_1$

Polymer	φ_1	φ_2	φ_3	φ_4	$M_{n,Ave}$ (kg mol^{-1})	$Đ_{Ave}$	$M_{n,1}$ (kg mol^{-1})	$Đ_1$
$PFPE_{D10}$–Diol	1	0	0	0	1.0	1.07	1.0	—
$PFPE_{D10}$–DMC	1	0	0	0	1.1	1.05	1.1	—
$PFPE_{E10}$–Diol	0.88	0.09	0.03	0	1.5	1.1	1.3	1.03
$PFPE_{E10}$–DMC	0.43	0.25	0.05	0.27	1.9	1.3	1.5	1.03

Experimental section

Materials

The polymer $PFPE_{D10}$–Diol was purchased from Santa Cruz Biotechnology and $PFPE_{E10}$–Diol was purchased from Solvay-Solexis. The polymers $PFPE_{D10}$–DMC and $PFPE_{E10}$–DMC were synthesized from the respective diols. The synthesis and characterization of the dimethyl carbonate polymers were reported previously.[8,20] As a reference, a low molecular weight liquid PEO was also studied. PEO was purchased from Polymer Source and the number-averaged molecular weight, M_n, of the PEO was 400 g mol^{-1}. All materials were dried prior to use at room temperature for 72 h under vacuum in a glovebox antechamber. Subsequently, the materials were handled in an Ar glovebox with a water level below 1 ppm and an O_2 level below 5 ppm, or they were sealed in air-tight sample holders.

The structures of the polymers used in this study, $PFPE_{D10}$–Diol, $PFPE_{D10}$–DMC, $PFPE_{E10}$–Diol, and $PFPE_{E10}$–DMC are shown in Table 1. The PFPE chains are random copolymers of CF_2CF_2O, tetrafluoroethylene oxide (TFEO), and CF_2O, difluoromethylene oxide (DFMO), and the average ratios of these components, m and n, taken from ref. 20, are given in Table 1.[20] In the $PFPE_{E10}$ polymers, the average number of EO units per chain is given by $2q$. In ref. 20, a combination of mass spectrometry, nuclear magnetic spectroscopy, and gel permeation chromatography was used to elucidate the structures of the PFPE polymers. The $PFPE_{D10}$ materials were reported to have unimodal molecular weight distributions, while both the as-received and DMC-modified $PFPE_{E10}$ materials exhibited chain coupling. The characteristics of the molecular weight distributions are reported in Table 2.

Wide angle X-ray scattering

Samples for the WAXS experiments were prepared in a glovebox and sealed in airtight aluminum cells. To mount the liquid samples, a 0.794 mm thick, chemically-resistant, fluoro-elastomer (tradename Aflas) spacer with a 3.175 mm diameter hole was placed on a 25 μm X-ray transmissive polyimide window. The polymer sample (6 μL) was dispensed into the hole, and a

second polyimide window was placed on top without trapping bubbles in the liquid sample. The samples were placed in airtight aluminum holders, which were mounted onto a home-built temperature controlled stage, up to 8 at a time. Measurements were taken between 30 °C and 90 °C, at intervals of 15 °C, after waiting 45 min at each temperature. The temperatures of the holders were monitored in an offline heating experiment and found to be within ±2 °C of the set temperature for every temperature and sample position in the heating stage.

Wide angle X-ray scattering (WAXS) experiments were performed at beamline 7.3.3 at the Advanced Light Source synchrotron in Berkeley, California, USA.[21] The X-ray energy was 10 keV, and the detector was a Pilatus 2 M camera from Dectris, with a pixel size of 0.172 × 0.172 mm. The incident beam intensity was measured using an ion gauge, and the transmitted intensity was measured using a photodiode on the beamstop. The scattering vector and the sample–detector distance were calibrated with a silver behenate standard using the first five Bragg diffraction peaks, and the sample–detector distance was determined to be 283 mm. An exposure time of 60 s was used for the polymer samples. Two-dimensional scattering patterns were azimuthally averaged and reduced to one-dimensional scattering profiles using the Nika package for IgorPro.[22]

Wide angle scattering profiles were corrected for scattering due to the polyimide windows and due to beam divergence, and the scattering intensity was calibrated as described in ref. 23. In the wide angle regime, the angle-dependent transmission of X-rays through the sample must be taken into account in background subtraction because X-rays scattered at wide angles travel a longer distance through the scattering object than X-rays scattered at smaller angles. In small angle scattering, this effect can be neglected. In addition, intensity due to beam spreading may contribute to the measured signal. To aid in the intensity calibration and background subtraction, WAXS profiles were obtained for air (1 s and 60 s exposures), a blank cell containing polyimide windows but no polymer sample (60 s exposure), and a 1 mm thick glassy carbon standard for intensity calibration (sample M13, Jan Ilavsky, 1 s exposure). Eqn (1), derived in ref. 23, gives the expression used for the background subtraction and beam spreading corrections.[23]

$$I_{\mathrm{corr}}(q) = \frac{1}{T_{\mathrm{w}} T_{\mathrm{s}}(\theta) T_{\mathrm{w}}^{\theta} T_{\mathrm{fp}}^{\theta}} \times \left\{ \begin{array}{l} [I_{\mathrm{sam}}(q) - \mathrm{DC}] - \dfrac{\left(T_{\mathrm{s}}^{\theta} T_{\mathrm{w}}^{\theta} + T_{\mathrm{w}} T_{\mathrm{s}}\right)}{\left(T_{\mathrm{w}}^{\theta} + T_{\mathrm{w}}\right)} [I_{\mathrm{ec}}(q) - \mathrm{DC}] \\ \quad - \left[T_{\mathrm{s}} - \dfrac{\left(T_{\mathrm{s}}^{\theta} T_{\mathrm{w}}^{\theta} + T_{w} T_{s}\right)}{\left(T_{\mathrm{w}}^{\theta} + T_{\mathrm{w}}\right)} \right] T_{\mathrm{w}}{}^{2} [I_{\mathrm{b}}(q) - \mathrm{DC}] \end{array} \right\} \quad (1)$$

Here, $I_{\mathrm{corr}}(q)$ is the corrected, measured scattering intensity due to the sample, T is the total transmission, $T(\theta)$ is the angle-dependent X-ray transmission for a moderately absorptive object (assuming no multiple-scattering events), T^{θ} is the path-length-corrected X-ray transmission, $I_{\mathrm{sam}}(q)$ is the uncorrected, measured sample intensity, DC is the dark current signal, $I_{\mathrm{ec}}(q)$ is the measured empty cell or polyimide blank cell intensity, and $I_{\mathrm{b}}(q)$ is the measured background or air intensity (60 s exposure). The subscript w represents one window, s represents the free-standing sample, and fp represents the post-sample flight path. The total transmission T is given by eqn (2), where μ is the linear absorption coefficient and z is the thickness of the scattering object.

$$T = \mathrm{e}^{-\mu z} \quad (2)$$

The angle-dependent transmission, $T(\theta)$ for a moderately absorbing, thick object (assuming no multiple scattering events) is defined by eqn (3).

$$T(\theta) \equiv T\left(\frac{T^{a(\theta)} - 1}{a(\theta)\ln(T)}\right); \quad a(\theta) = \frac{1}{\cos\theta} - 1 \quad (3)$$

Path-length-dependent transmission is defined by eqn (4).

$$T^{\theta} \equiv \mathrm{e}^{\left(\frac{-\mu z}{\cos\theta}\right)} = T^{\frac{1}{\cos\theta}} \quad (4)$$

In our experiments, since detectors with different mechanisms and gains are used to measure the beam intensity before and after the sample (ion chamber and photodiode), we do not directly measure the absolute transmission given by eqn (2). Instead we measure an apparent transmission $T^{\mathrm{Obs}} = I^{\mathrm{PD}}/I^{\mathrm{IC}}$, where I^{PD} is the measured response from the post-sample photodiode and I^{IC} is the measured response from the pre-sample ion chamber. The absolute transmissions can be estimated from these quantities by the following relationships (eqn (5)–(7)):

$$T_{\mathrm{s}} = T_{\mathrm{sam}}^{\mathrm{Obs}}/T_{\mathrm{ec}}^{\mathrm{Obs}} \quad (5)$$

$$T_{\mathrm{w}} = \left(\frac{T_{\mathrm{ec}}^{\mathrm{Obs}}}{T_{\mathrm{b}}^{\mathrm{Obs}}}\right)^{\frac{1}{2}} \quad (6)$$

$$T_{\mathrm{fp}}(T) \approx \frac{\mathrm{e}^{-\mu_{\mathrm{b}} z_{\mathrm{b}}}}{T_{\mathrm{b}}^{\mathrm{Obs}}(25\ ^{\circ}\mathrm{C})} T_{\mathrm{b}}^{\mathrm{Obs}}(T) \quad (7)$$

where $T_{\mathrm{sam}}^{\mathrm{Obs}}$ is the apparent transmission from the entire sample including windows, $T_{\mathrm{ec}}^{\mathrm{Obs}}$ is the apparent transmission from the polyimide blank cell, $T_{\mathrm{b}}^{\mathrm{Obs}}$ is the apparent transmission from air, μ_{b} is the linear absorption coefficient of dry air at 25 °C (5.65×10^{-3} cm^{-1}), and z_{b} is the sample–detector distance, 283 mm.[24] In eqn (6), the ratio of apparent transmissions is raised to the $\frac{1}{2}$ power to account for the presence of two polyimide films in the blank cell. In eqn (7), the transmission of the flight path is estimated as a function of temperature, T, since the density of the air around the heating stage varies with temperature. The apparent transmission at a given temperature is scaled by the quotient of the theoretical transmission at 25 °C (from the literature) and the apparent transmission at 25 °C.[24]

A constant intensity calibration factor was determined using a glassy carbon standard.[25] The measured intensity was corrected for beam spreading by subtracting the scattering from air according to eqn (8).

$$I_{\mathrm{corr}}(q) = \frac{1}{T_{\mathrm{s}}(\theta) T_{\mathrm{fp}}^{\theta}} \times \{[I_{\mathrm{sam}}(q) - \mathrm{DC}] - T_{\mathrm{s}}[I_{\mathrm{b}}(q) - \mathrm{DC}]\} \quad (8)$$

In this case, the sample is glassy carbon without polyimide windows, and the scattering from the sample, $I_{sam}(q)$, and air, $I_b(q)$, were measured using a 1 s exposure. A constant calibration factor was determined by scaling the measured, corrected scattering profile from glassy carbon to match the known absolute scattering profile from the M13 glassy carbon sample.

Results

In Fig. 1a, scattering profiles are shown for the PFPE and PEO polymers at 30 °C. The block copolymers $PFPE_{E10}$–Diol and $PFPE_{E10}$–DMC have a peak in the vicinity of $q_1 \approx 2$ nm^{-1}, which is not present in the profiles of the pure PFPE or PEO polymers. Because the q_1 peak is present only in the block copolymers, we attribute it to fluctuations between the PEO-rich and PFPE-rich phases. The peak is broad and similar to that observed in the disordered block copolymers. Fig. 1b shows the temperature dependence of the scattering profiles for $PFPE_{E10}$–Diol. The temperature-dependent scattering of the other polymers is included in the ESI.† Fig. 1c shows the temperature-dependence of the q_1 peak in the $PFPE_{E10}$–Diol polymer in more detail. The intensity of the q_1 peak decreases with temperature, and the peak shifts to higher values of q.

In Fig. 1a, all polymers, both $PFPE_{E10}$ block copolymers and $PFPE_{D10}$ and PEO single-phase polymers, show two similar peaks, one in the vicinity of $q_2 \approx$ 12–15 nm^{-1}, and one in the vicinity of $q_3 \approx 30$ nm^{-1}. These correspond to characteristic spacings, $d = 2\pi/q$, of $d_2 \approx$ 0.4–0.5 nm and $d_3 \approx 0.2$ nm. Peaks such as q_2 and q_3 are sometimes called amorphous halos. The q_2 peak is at significantly different positions between the PFPE-containing polymers and pure PEO, while the q_3 peak is at similar positions for all of the polymers. The position of the maximum of the q_2 peak, $q_{2,max}$, is reported for the PFPE polymers as a function of temperature in Fig. 2. The effect of temperature on the q_2 and q_3 peaks in $PFPE_{E10}$–Diol is qualitatively similar to that in the other polymers (Fig. 1b, 2 and Fig. S1 in the ESI†). The intensities of the q_2 and q_3 peaks remain relatively constant with temperature. With increasing temperature, the q_2 peak shifts to lower q, and the q_3 peak remains nearly constant. The small feature at $q \approx 4$ nm^{-1}, which is apparent in all the scattering profiles in Fig. 1, is an artifact from the subtraction of scattering from polyimide windows.

The value of d_2 and the fact that $q_{2,max}$ is temperature-dependent suggest that it reflects the average distance between adjacent chains. The value of d_3 and the fact that peak q_3 is temperature independent suggests that it reflects bond distances along the polymer chains. In Fig. 2, the value of $q_{2,max}$ is slightly higher for the DMC-terminated polymers than the diol-terminated ones, suggesting that for the DMC-terminated polymers, the chain packing is slightly denser. We attribute this to hydrogen bonding in the diol-terminated polymers. For PEO, the value of $q_{2,max}$ ranges from 14.8–15.2 nm^{-1}. These values are considerably higher than the values for the PFPE polymers presented in Fig. 2, indicating that the average distance between adjacent PFPE chains is larger than that of PEO chains. We attribute this to the fact that the Van der Waals cross-section of fluorinated chains is larger than that of their hydrogenated counterparts.[26]

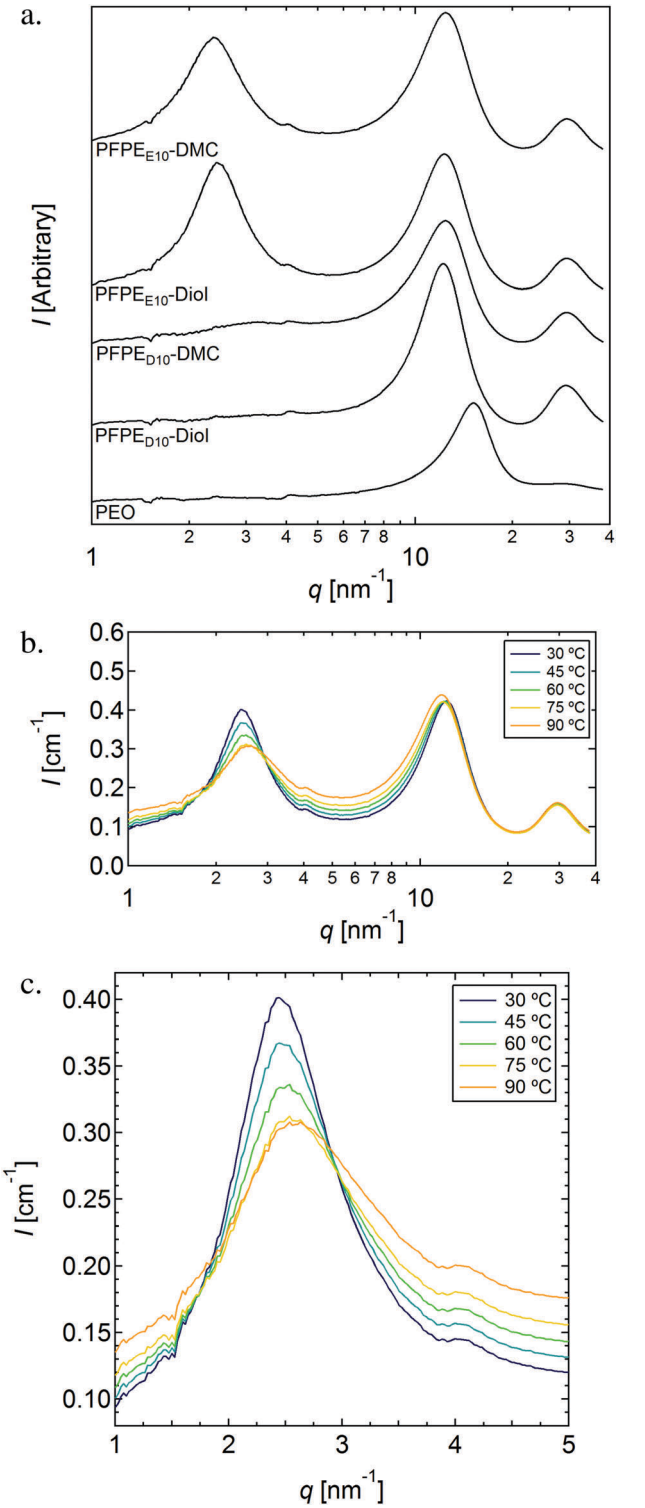

Fig. 1 In (a), WAXS profiles of the PFPE and PEO polymers are shown at 30 °C. Traces are offset for clarity. In (b), intensity-calibrated WAXS profiles are shown for the polymer $PFPE_{E10}$–Diol at temperatures ranging from 30 to 90 °C. In (c), the first peak of the $PFPE_{E10}$–Diol scattering profiles is shown in more detail.

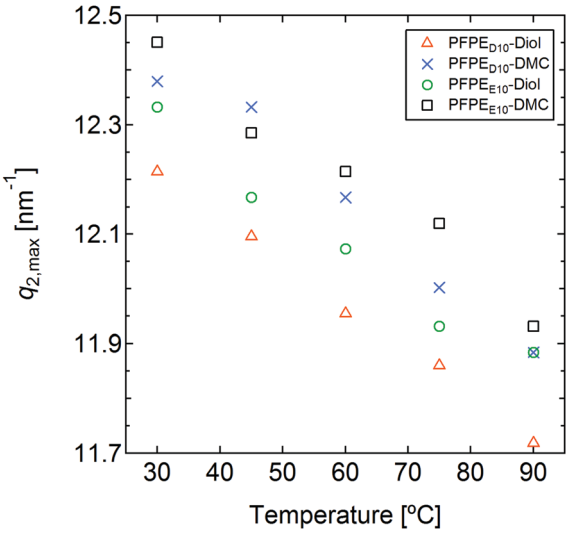

Fig. 2 The position of the maximum of the second scattering peak, $q_{2,max}$, is shown for the PFPE polymers as a function of temperature.

The q_1 peak in the block copolymer scattering profiles can be used to determine the interaction parameter between the PFPE and PEO blocks, as well as the radius of gyration, R_g, of the chain. Given the multimodal molecular weight distributions of the PFPE$_{E10}$ materials (see Table 2), a multiblock RPA model is used. Based on the RPA theory of Leibler, the scattering due to a monodisperse disordered block copolymer is given by eqn (9).[13,27]

$$I_{dis}(q) = v_{ref}\left(\frac{b_A}{v_A} - \frac{b_B}{v_B}\right)^2\left[\frac{1}{N}\frac{S(q)}{W(q)} - 2\chi\right]^{-1} \quad (9)$$

Here, $I_{dis}(q)$ is the disordered scattering intensity, v_{ref} is a reference volume taken to be 0.1 nm^3 in this study, b_i is the scattering length of block i, v_i is the monomer volume for block i, and $S(q)$ and $W(q)$ are the sum and determinant of the structure factor matrix, $[S_{ij}]$. The scattering length, b_{PFPE}, of the PFPE block was calculated by taking the average of the scattering lengths of the TFEO and DFMO monomers, weighted by the coefficients m and n, given in Table 1. We neglect any scattering contribution from the diol or DMC end groups. The monomer volumes were calculated by eqn (10),

$$v_i = \frac{M_i}{\rho_i N_{Av}} \quad (10)$$

where M_i is the molar mass of the monomer, ρ_i is the bulk density of the pure PEO or PFPE phase, and N_{Av} is Avagadro's number. The values for M_i used in this study are 44.05 g mol^{-1} for EO, and 93.79 g mol^{-1} for PFE, the weighted average of the masses of the TFEO and DFMO monomers. The values for density used in this study are 1.12 g cm^{-3} for EO, based on the relationship 1.139 [g cm^{-3}] − 7.31 × 10^{-4} [g cm^{-3} °C^{-1}] × T at 30 °C, and 1.77 g cm^3 for PFPE, based on the manufacturer's data on the density of PFPE$_{D10}$–Diol.[28] The scattering contrast, c, is defined by the prefactor in eqn (9) (eqn (11)). For the PFPE$_{E10}$ polymers, the theoretical value is c_{th} = 0.17 cm^{-1}.

$$c \equiv v_{ref}\left(\frac{b_A}{v_A} - \frac{b_B}{v_B}\right)^2 \quad (11)$$

To account for the polydispersity of our samples, we regard the samples as mixtures of monodisperse, coupled components. The scattering of the mixture, $I_{dis,mix}(q)$, is taken to be the sum of scattering from each coupled component, $I_{dis,k}(q)$, weighted by the volume fraction of the component, φ_k (eqn (12)). Here, component k consists of k chains, with k = 1 being the uncoupled chain.

$$I_{dis,mix}(q) = \sum_{k=1}^{4} \varphi_k \times I_{dis,k}(q) \quad (12)$$

The scattering of each component, $I_{dis,k}(q)$ is calculated according to eqn (9), where RPA is used to calculate $[S_{ij}]_k$, $S_k(q)$ and $W_k(q)$ for each component by treating component 1 as an ABA triblock, component 2 as an ABABA pentablock, component 3 as an ABABABA heptablock, and component 4 as an ABABABABA nonablock.[29] The expressions for $S_k(q)$ and $W_k(q)$ are given in eqn (13)–(16).

$$S_k(q) = g_{AA,k}(x) + 2g_{AB,k}(x) + g_{BB,k}(x) \quad (13)$$

$$W_k(q) = g_{AA,k}(x)g_{BB,k}(x) - [g_{AB,k}(x)]^2 \quad (14)$$

$$g_{AB,k}(x) = g_{BA,k}(x) \quad (15)$$

$$x \equiv q^2 {R_{g,1}}^2 \quad (16)$$

Here, $g_{AB,k}(x)$, $g_{AA,k}(x)$, and $g_{BB,k}(x)$ represent the elements of the structure factor matrix $[S_{ij}]_k$. Expressions for these terms depend on the block architecture, and are given in the supporting information for both uncoupled and coupled polymers, k = 1–4. The expressions for $S_k(q)$, $W_k(q)$, and hence $I_{dis,k}(q)$, depend on the radius of gyration and degree of polymerization of each component, $R_{g,k}$ and N_k, and the volume fraction of the PFPE block, ϕ_{PFPE}, which is the same for every component. The values $R_{g,k}$ and N_k can be expressed in terms of $R_{g,1}$ and N_1, the values for the uncoupled component (eqn (17) and (18)), by assuming a Gaussian chain. The radius of gyration can also be expressed in terms of the statistical segment length, l.

$$R_{g,k} = \sqrt{k}R_{g,1} = \sqrt{\frac{kN_1}{6}}l \quad (17)$$

$$N_k = kN_1 \quad (18)$$

The degree of polymerization, N_1, calculated from eqn (19) and (20), is 10.5.[30]

$$N_1 = N_{PEO} + N_{PFPE} \quad (19)$$

$$N_i = \frac{\hat{N}_i v_i}{v_{ref}} \quad (20)$$

Here, $\hat{N}_i$ is the number of monomers in an uncoupled chain, $2q$ for EO and $m + n$ for PFE (Table 1). The volume fraction of PFPE, ϕ_{PFPE}, given by eqn (21), is 0.75.

$$\phi_{PFPE} = \frac{v_{PFE}}{v_{PFE} + \frac{\hat{N}_{i,PEO}}{\hat{N}_{i,PFPE}}v_{EO}} \quad (21)$$

From Fig. 1b and c, it is apparent that the q_2 peak and a temperature-dependent background contribute to the disordered scattering intensity at the q_1 peak. There are several phenomena

that contribute to background scattering in the WAXS regime, including thermal density fluctuations, incoherent scattering, and Compton scattering.[31,32] These contributions are not removed by the empty cell background subtraction, and it is difficult to account for all of them using fundamental models. Motivated by the work of Vonk *et al.*, we fit the background, $I_{bg}(q)$, with a constant, a_0, and a Lorentzian due to the contribution of q_2 (eqn (22)).[31–33]

$$I_{bg}(q) = a_0 + \frac{a_1}{(q - q_{2,max})^2 + a_2} \quad (22)$$

Here, a_0, a_1, and a_2 are adjustable parameters, and $q_{2,max}$ is the scattering vector at the maximum of the q_2 peak, given in Fig. 2.

The values of $R_{g,1}$ and χ are determined by fitting the model for the total scattering intensity, $I_{tot}(q)$, (eqn (23)) to the scattering profiles for $PFPE_{E10}$–Diol and $PFPE_{E10}$–DMC.

$$I_{tot}(q) = I_{bg}(q) + I_{dis,mix}(q) \quad (23)$$

The term $I_{dis,mix}(q)$ can be fit by as few as two adjustable parameters, $R_{g,1}$ and χ. Due to our lack of knowledge of the density of the PFPE block as a function of temperature, in some fits, the contrast c is used as an additional fit parameter. For the values of $R_{g,1}$ and χ reported herein, $I_{tot}(q)$ is fit using six parameters, $R_{g,1}$, χ, c, a_0, a_1, and a_2, in the q range of 1–10 nm^{-1}. The values of $R_{g,1}$ and χ, determined using the fixed value of $c = 0.17$ cm^{-1}, are reported in the ESI.† The values of $R_{g,1}$ and χ are similar between fits with c as an adjustable or fixed parameter. The other fixed parameters used in the model (eqn (22)) are summarized in Table 3.

An example of the fitting procedure is shown in Fig. 3a, where data from $PFPE_{E10}$–Diol at 30 °C are analyzed. It is evident that $I_{tot}(q)$ is in quantitative agreement with the experimental data. The two contributions to $I_{tot}(q)$, $I_{dis,mix}(q)$, and $I_{bg}(q)$, are also shown in Fig. 3a. The scattering intensity due to disordered fluctuations $I_d(q)$ is defined in eqn (24).

$$I_d(q) = I(q) - I_{bg}(q) \quad (24)$$

In Fig. 3b, we show the q-dependence of the scattering data, I_d, and that of the multicomponent RPA, $I_{dis,mix}(q)$, as a function of temperature for $PFPE_{E10}$–Diol. It is interesting to note that the $I_d(q)$ data in Fig. 3 are qualitatively similar to the data obtained from typical disordered block copolymers, in spite of the qualitative differences in the data reduction procedures.[14,15,17–19]

The values of $R_{g,1}$ and χ, determined by fitting eqn (23) to the scattering data, are shown in Fig. 4. The values of the fit parameters a_0, a_1, and a_2 are given in the ESI.† For both $PFPE_{E10}$–Diol and $PFPE_{E10}$–DMC, $R_{g,1} \sim 1$ nm and decreases with temperature, as for most block copolymers. The corresponding values of l (eqn (12)) are

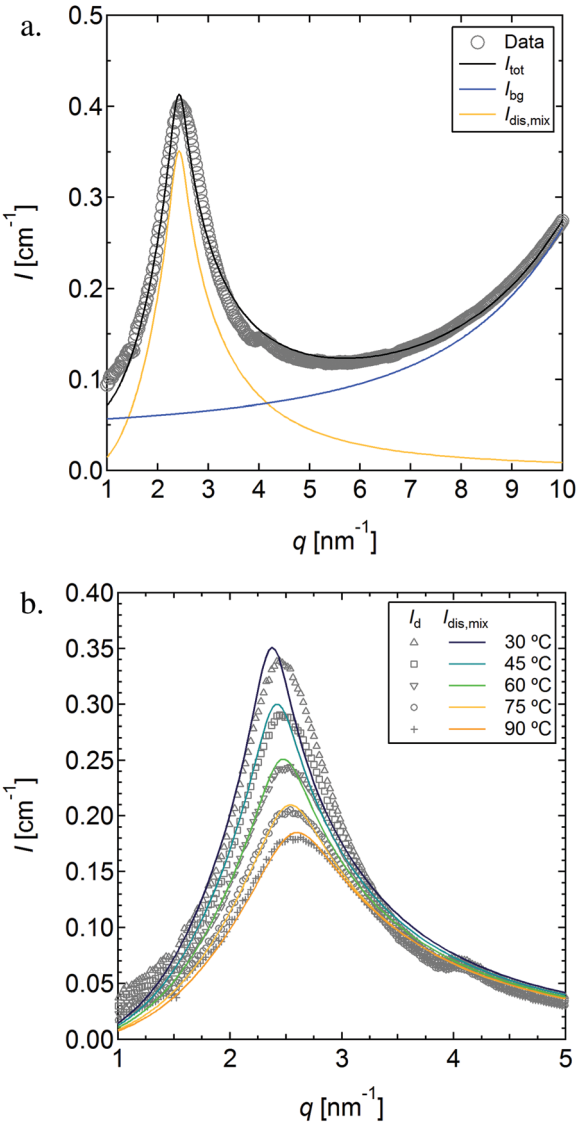

Fig. 3 Comparison of fits based on the random phase approximation (RPA) model and experimental wide angle X-ray scattering data. In (a), an experimental scattering profile from $PFPE_{E10}$–Diol at 30 °C is shown along with the fit to the RPA model, I_{tot}. The components of the fit from disordered scattering, $I_{dis,mix}$, and the background, I_{bg}, are also shown. In (b), disordered scattering is shown for $PFPE_{E10}$–Diol as a function of temperature. The markers represent $I_d(q)$, the difference between the experimental data and the background component of the fit, I_{bg}, and the solid lines represent the fit component, $I_{dis,mix}$.

in the vicinity of 0.8–0.9 nm, close to the values published by Cotts for various copolymers consisting of EO, TFEO and DFMO segments.[34] In the work of Cotts, values of l of 0.8 to 1.0 nm were obtained by intrinsic viscosity measurements in conjunction

Table 3 Fixed parameters used in the random phase approximation model. The parameters given below are the scattering lengths, b_i, monomer molar masses, M_i, densities, ρ_i, monomer volumes, v_i, reference volume, v_{ref}, theoretical contrast, c_{th}, degree of polymerization, N_1, and volume fraction of PFPE, ϕ_{PFPE}

b_{PEO} (nm)	b_{PFPE} (nm)	M_{EO} (g mol^{-1})	M_{PFE} (g mol^{-1})	ρ_{PEO} (g cm^{-3})	ρ_{PFPE} (g cm^{-3})	v_{EO} (nm^3)	v_{PFE} (nm^3)	v_{ref} (nm^3)	c_{th} (cm^{-1})	N_1	ϕ_{PFPE}
6.76×10^{-5}	1.28×10^{-4}	44.05	93.79	1.12	1.77	6.53×10^{-2}	8.80×10^{-2}	0.1	0.17	10.5	0.75

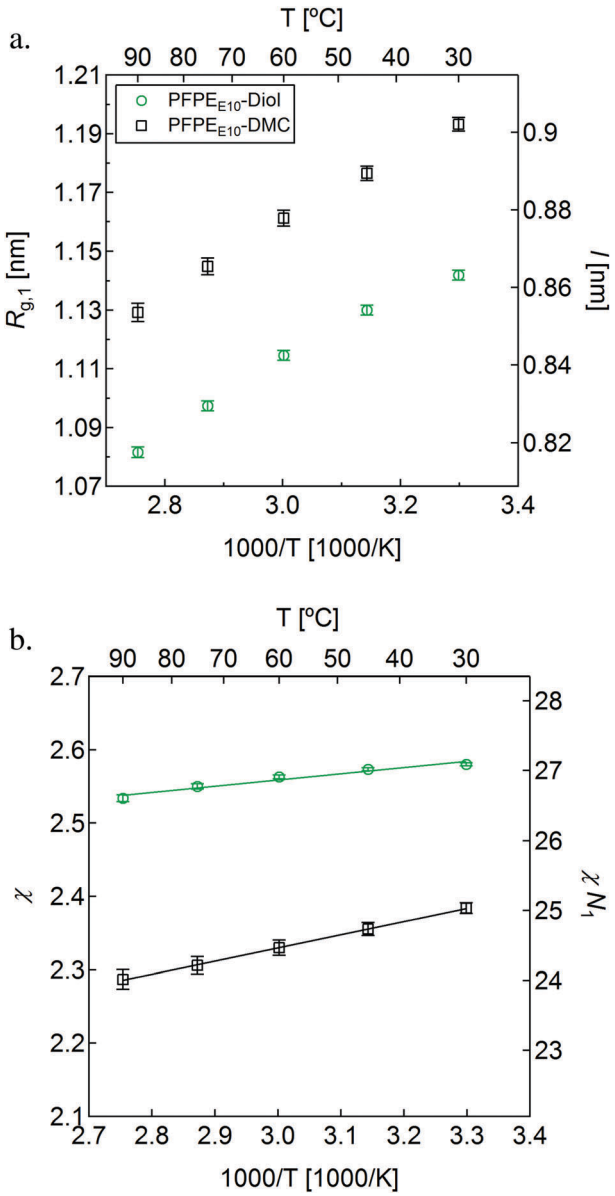

Fig. 4 Random phase approximation parameters. In (a), the radius of gyration and statistical segment length, $R_{g,1}$ and l, are given for PFPE$_{E10}$–Diol and PFPE$_{E10}$–DMC as a function of temperature. In (b), the interaction parameter, χ, is shown. The lines through the data in (b) represent fits to eqn (25). The quantity χN_1 is also given for reference. The error bars give the uncertainty in $R_{g,1}$ and χ from the RPA fit to the scattering data.

with a worm-like chain model.[34,35] The value of $R_{g,1}$ is slightly larger for PFPE$_{E10}$–DMC than for PFPE$_{E10}$–Diol.

Fig. 4b shows the temperature dependence of χ. The solid lines are fits based on eqn (25). In Table 4, the values of A and B are reported for both RPA models, the model with c as a variable parameter corresponding to the data reported in Fig. 4, and the model with fixed $c = c_{th} = 0.17$ cm^{-1}, corresponding to the data reported in the ESI† (Fig. S2).

$$\chi(T) = A + \frac{B}{T} \tag{25}$$

Table 4 Temperature dependence of interaction parameter χ. The parameters A and B defined in eqn (23) are given below for values of χ calculated by the RPA models with varying contrast parameter, c, and fixed c. The data supporting the RPA model with fixed c are reported in the ESI

	RPA with variable c		RPA with fixed c	
Polymer	A	B [K]	A	B [K]
PFPE$_{E10}$–Diol	2.3	84	2.3	106
PFPE$_{E10}$–DMC	1.8	180	1.2	355

From Table 4, it is evident that the magnitude of χ determined using the variable c model is comparable to the magnitude of χ determined using the fixed c model, over the temperature range studied. In the fixed c model, χ is a stronger function of temperature because all of the temperature dependence is accounted for by the χ parameter. In the variable c model, χ is a slightly weaker function of temperature because c and χ are both allowed to vary with temperature. In both models, the values of χ are lower for PFPE$_{E10}$–DMC than for PFPE$_{E10}$–Diol, suggesting that end groups may play a role in miscibility; however, we have not directly considered the effects of the end groups on χ in this study.[36,37]

The high values of χ in the PFPE$_{E10}$ polymers indicate low miscibility between the PEO and PFPE blocks (see Fig. 4b). The values of χ for the PFPE–PEO block copolymers are much higher compared to those for hydrogenated PEO-containing block copolymers, for example polystyrene-*block*-poly(ethylene oxide) (SEO).[27,38,39] Cochran *et al.* found a value of $\chi = 0.075$ for SEO of 150 kg mol^{-1} at 30 °C, and Zhu *et al.* found a similar value of $\chi = 0.063$ for SEO of 18 kg mol^{-1} at 30 °C. High χ values have also been reported in other block copolymers with fluorinated and non-fluorinated segments.[40–42]

In ref. 43, the miscibility between PFPE$_{D10}$–Diol and PEO with similar degrees of polymerization ($N_{PFPE} = 9.5$ and $N_{PEO} = 5.9$, based on eqn (20)) was studied at room temperature.[43] Blends with a PEO volume fraction of less than 40 wt% were miscible while blends with a PEO volume fraction greater than 40 wt% were immiscible. This kind of asymmetric behavior is inconsistent with the Flory–Huggins theory. Based on the χ parameter that we obtained for PFPE$_{E10}$–Diol at 30 °C, these homopolymer blends would be predicted to be immiscible over a wide range of PEO volume fractions; χN_{Ave} is 19.0 where N_{Ave} is defined in eqn (26).

$$N_{Ave} = \frac{4}{\left(\frac{1}{\sqrt{N_{PFPE}}} + \frac{1}{\sqrt{N_{PEO}}}\right)^2} \tag{26}$$

For miscible blends, χN_{Ave} must be less than 2. Further work is needed to reconcile the differences between the block copolymer and blend thermodynamics in PFPE–PEO systems. Such discrepancies between the block copolymer and homopolymer blends have been noted in the literature.[44,45]

The extent to which the RPA analysis applies to chains as short as those used in this study remains unknown. We use this framework mainly due to the lack of better alternatives for disordered systems. A previous study that examined short diblock copolymers used the same framework to determine χ.[27]

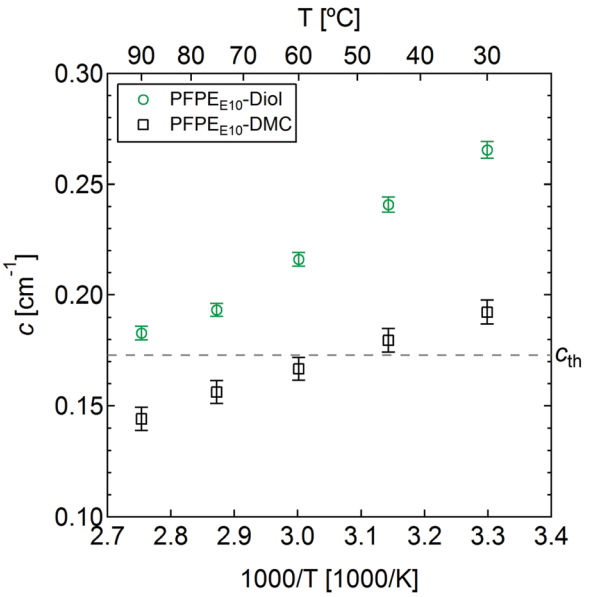

Fig. 5 The contrast term, c, is shown as a function of temperature. The dashed line represents the theoretical contrast value, c_{th} = 0.17 cm^{-1}. The error bars give the uncertainty in c from the RPA fit to the scattering data.

Other studies on short diblock copolymers used order–disorder transition temperatures and domain spacings in microphase-separated systems to estimate χ.[41,46–50] The onset of microphase separation is expected to occur in the vicinity of the temperature at which the scattering intensity at $q_{1,max}$ diverges. This divergence occurs at $(\chi N)_{critical}$ = 27.51 for PFPE$_{E10}$–Diol, and $(\chi N)_{critical}$ = 26.93 for PFPE$_{E10}$–DMC. Based on the temperature-dependence of χ, we expect microphase separation at temperatures below 262 K for PFPE$_{E10}$–Diol and 235 K for PFPE$_{E10}$–DMC. The values of χN_1 obtained in the temperature range studied are close to the critical values (see Fig. 4b). The estimate of the transition temperature may be improved by using a fluctuation-corrected theory such as that by Fredrickson and Helfand.[16] Experimental and theoretical work has shown that χ generally decreases as the chain length increases.[18,27,51] The values of χ obtained herein are likely higher than those that would be obtained for long chain PFPE–PEO block copolymers.

Fig. 5 shows the temperature dependence of the fit contrast term, c. Also shown in Fig. 5 is the calculated value of c, c_{th} (dashed line). The contrast in our experiments is due to the electron density difference between the A and B segments, as indicated by eqn (11). The values of c determined by fitting are similar to the theoretical value c_{th} = 0.17 (dashed line in Fig. 5). For both polymers, c decreases with temperature, indicating that the temperature-dependence of the density of PFPE is stronger than that of PEO. The fitted value of c is higher for PFPE$_{E10}$–Diol than for PFPE$_{E10}$–DMC, consistent with the fact that the electron-rich DMC end group reduces the electron density difference between the PEO and PFPE blocks.

Conclusion

We have studied the thermodynamic interactions in short chain, commercial PFPE–PEO block copolymers. Because of the short chain lengths, WAXS was used to probe disordered concentration fluctuations. New data reduction procedures that enable the determination of absolute WAXS intensity are presented. The presence of coupled products in the commercial samples was accounted for by the use of the multicomponent RPA. Theoretical RPA fits through the experimental data were used to determine the Flory–Huggins interaction parameter and the radius of gyration of the polymers χ and $R_{g,1}$. Our ability to detect concentration fluctuations was enabled by both a relatively large value of χ and significant scattering contrast. The presence of heterogeneity on the nanometer length scale detected in this work cannot be inferred from previous studies of these commercially-important materials. Our work thus far is limited to the disordered state. The ordered state may be accessed by either decreasing the temperature or increasing the chain length. We hope to expand the experimental window in future studies to access ordered morphologies in these systems.

Author contributions

The manuscript was written through contributions of all authors. All authors have given approval to the final version of the manuscript.

Funding sources

U. S. Department of Energy, DE-SC0012673.

Competing financial interests

The authors declare no competing financial interests.

Acknowledgements

This work was supported as part of the Center for Mesoscale Transport Properties, an Energy Frontier Research Center supported by the U.S. Department of Energy, Office of Science, Basic Energy Sciences, under award #DE-SC0012673. The wide angle X-ray scattering was performed at beamline 7.3.3 at the Advanced Light Source synchrotron in Berkeley, California, USA. Beamline 7.3.3 is supported by the Director of the Office of Science, Office of Basic Energy Sciences, of the U.S. Department of Energy under Contract No. DE-AC02-05CH11231.

References

1 M. J. R. Cantow, R. B. Larrabee, E. M. Barrall II, R. S. Butner, P. Cotts, F. Levy and T. Y. Ting, Molecular Weights and Molecular Dimensions of Perfluoropolyether Fluids, *Macromol. Chem. Phys.*, 1986, **187**(10), 2475–2481.
2 L. Holland, L. Laurenson, P. N. Baker and H. J. Davis, Perfluoropolyether—a Vacuum Pump Fluid Resistant to Electron Induced Polymerization, *Nature*, 1972, **238**, 36–37.

3 G. Caporiccio, F. Burzio, G. Carniselli and V. Biancardi, Some Physicochemical Properties of Perfluoropolyether Surfactants, *J. Colloid Interface Sci.*, 1984, **98**(1), 202–209.
4 J. C. Yarbrough, J. P. Rolland, J. M. DeSimone, M. E. Callow, J. A. Finlay and J. A. Callow, Contact Angle Analysis, Surface Dynamics, and Biofouling Characteristics of Cross-Linkable, Random Perfluoropolyether-Based Graft Terpolymers, *Macromolecules*, 2006, **39**, 2521–2528.
5 Z. Hu, J. A. Finlay, L. Chen, D. E. Betts, M. A. Hillmyer, M. E. Callow, J. A. Callow and J. M. Desimone, Photochemically Cross-Linked Perfluoropolyether-Based Elastomers: Synthesis, Physical Characterization, and Biofouling Evaluation, *Macromolecules*, 2009, **42**(18), 6999–7007.
6 Y. Wang, L. M. Pitet, J. A. Finlay, L. H. Brewer, G. Cone, D. E. Betts, M. E. Callow, J. A. Callow, D. E. Wendt, M. A. Hillmyer and J. M. DeSimone, Investigation of the Role of Hydrophilic Chain Length in Amphiphilic Perfluoropolyether/poly(ethylene Glycol) Networks: Towards High-Performance Antifouling Coatings, *Biofouling*, 2011, **27**(10), 1139–1150.
7 E. Molena, C. Credi, C. De Marco, M. Levi, S. Turri and G. Simeone, Protein Antifouling and Fouling-Release in Perfluoropolyether Surfaces, *Appl. Surf. Sci.*, 2014, **309**, 160–167.
8 D. H. C. Wong, J. L. Thelen, Y. Fu, D. Devaux, A. A. Pandya, V. S. Battaglia, N. P. Balsara and J. M. DeSimone, Nonflammable Perfluoropolyether-Based Electrolytes for Lithium Batteries, *Proc. Natl. Acad. Sci. U. S. A.*, 2014, **111**(9), 3327–3331.
9 A. K. P. Johnston, K. L. Harrison, M. J. Clarke, S. M. Howdle, M. P. Heitz, C. Carlier and T. W. Randolph, Water-in-Carbon Dioxide Microemulsions: An Environment for Hydrophiles Including Proteins, *Science*, 1996, **271**(5249), 624–626.
10 H. Abroshan, N. R. Dhumal, Y. Shim and H. J. Kim, Theoretical Study of Interactions of a $Li^{+}(CF_3\ SO_2)_2\ N^{-}$ Ion Pair with $CR_3\ (OCR_2CR_2)_nOCR_3$ (R = H or F), *Phys. Chem. Chem. Phys.*, 2016, **18**(9), 6754–6762.
11 M. W. Matsen, The Standard Gaussian Model for Block Copolymer Melts, *J. Phys.: Condens. Matter*, 2002, **14**, 20–47.
12 F. S. Bates and G. H. Fredrickson, Block Copolymer Thermo dynamics: Theory and Experiment, *Annu. Rev. Phys. Chem.*, 1990, **41**, 525–557.
13 L. Leibler, Theory of Microphase Separation in Block Copolymers, *Macromolecules*, 1980, **13**(6), 1602–1617.
14 R. J. Roe, M. Fishkis and J. C. Chang, Small-Angle X-Ray Diffraction Study of Thermal Transition in Styrene-Butadiene Block Copolymers, *Macromolecules*, 1981, **14**, 1091–1103.
15 T. Hashimoto, M. Shibayama and K. Hiromichi, Ordered Structure in Block Polymer Solutions. 4. Scaling Rules on Size of Fluctuations with Block Molecular Weight, Concentration, and Temperature in Segregation and Homogeneous Regimes, *Macromolecules*, 1983, **16**(7), 1093–1101.
16 G. H. Fredrickson and E. Helfand, Fluctuation Effects in the Theory of Microphase Separation in Block Copolymers, *J. Chem. Phys.*, 1987, **87**(1), 697–705.
17 F. S. Bates and M. A. Hartney, Block Copolymers near the Microphase Separation Transition. 3. Small-Angle Neutron Scattering Study of the Homogeneous Melt State, *Macromolecules*, 1985, **18**(12), 2478–2486.
18 C. C. Lin, S. V. Jonnalagadda, P. K. Kesani, H. J. Dai and N. P. Balsara, Effect of Molecular Structure on the Thermodynamics of Block Copolymer Melts, *Macromolecules*, 1994, **27**(26), 7769–7780.
19 D. Y. Ryu, U. Jeong, D. H. Lee, J. Kim, H. S. Youn and J. K. Kim, Phase Behavior of Deuterated Polystyrene-*Block*-Poly(*N*-Pentyl Methacrylate) Copolymers, *Macromolecules*, 2003, 2894–2902.
20 K. R. Olson, D. H. C. Wong, M. Chintapalli, K. Timachova, R. Janusziewicz, W. F. M. Daniel, S. Mecham, S. Sheiko, N. P. Balsara and J. M. DeSimone, Liquid Perfluoropolyether Electrolytes with Enhanced Ionic Conductivity for Lithium Battery Applications, *Polymer*, 2016, **100**, 126–133.
21 A. Hexemer, W. Bras, J. Glossinger, E. Schaible, E. Gann, R. Kirian, A. MacDowell, M. Church, B. Rude and H. Padmore, A SAXS/WAXS/GISAXS Beamline with Multilayer Monochromator, *J. Phys.: Conf. Ser.*, 2010, **247**, 12007.
22 J. Ilavsky, Nika: Software for Two-Dimensional Data Reduction, *J. Appl. Crystallogr.*, 2012, **45**(2), 324–328.
23 J. L. Thelen, S. Inceoglu, X. C. Chen and N. P. Balsara, Influence of Miscibility on Poly(ethylene oxide) Crystallization from Disordered Melts of Block Copolymers with Lithium and Magnesium Counterions, submitted for publication.
24 J. H. Hubbell and S. M. Seltzer, X-Ray Mass Attenuation Coefficients, *NIST Internal/Interagency Report* 5632, National Institute of Standards and Technology, Gaithersburg, MD, 1996.
25 F. Zhang, J. Ilavsky, G. G. Long, J. P. G. Quintana, A. J. Allen and P. R. Jemian, Glassy Carbon as an Absolute Intensity Calibration Standard for Small-Angle Scattering, *Metall. Mater. Trans. A*, 2009, **41**(5), 1151–1158.
26 A. A. Askadskii, Packing of Macromolecules and Polymer Density, *Computational Materials Science of Polymers*, Cambridge International Science Publishing, Cambridge, UK, 2003.
27 A. A. Teran and N. P. Balsara, Thermodynamics of Block Copolymers With and Without Salt, *J. Phys. Chem. B*, 2014, **118**(1), 4–17.
28 R. A. Orwoll, Physical Properties of Polymers Handbook in *Physical Properties of Polymers Handbook*, ed. J. E. Mark, Springer, New York, 2007, pp. 94–95.
29 S. Woloszczuk and M. Banaszak, Effects of Compositional Asymmetry in Phase Behavior of ABA Triblock Copolymer Melts from Monte Carlo Simulation, *Eur. Phys. J. E: Soft Matter Biol. Phys.*, 2010, **33**, 343–350.
30 H. B. Eitouni and N. P. Balsara, Thermodynamics of Polymer Blends, in *Physical Properties of Polymers Handbook*, ed. J. E. Mark, Springer, New York, 2007, pp. 339–359.
31 N. Stribeck, *X-Ray Scattering of Soft Matter*, Springer, New York, NY, 2007.
32 R. J. Roe, *Methods of X-Ray and Neutron Scattering in Polymer Science*, Oxford University Press, New York, NY, 2000.
33 C. G. Vonk, Investigation of Non-Ideal Two-Phase Polymer Structures by Small-Angle X-Ray Scattering, *J. Appl. Crystallogr.*, 1973, **6**(2), 81–86.

34 P. M. Cotts, Solution Properties of a Group of Perfluoropolyethers: Comparison of Unperturbed Dimensions, *Macromolecules*, 1994, **27**, 6487–6491.
35 M. Bohdanecký, New Method for Estimating the Parameters of the Wormlike Chain Model from the Intrinsic-Viscosity of Stiff-Chain Polymers, *Macromolecules*, 1983, **16**(9), 1483–1492.
36 C. Qian, S. Grigoras and L. D. Kennan, End Group Effects on the Phase Behavior of Polymer Blends: Poly(dimethylsiloxane) and Poly(methylphenylsiloxane) Blend, *Macromolecules*, 1996, **29**(4), 1260–1265.
37 J. H. Ryu and P. D. Gujrati, Lattice Theory of Polymer Solutions with Endgroup Effects, *J. Chem. Phys.*, 1997, **107**(4), 1259–1268.
38 E. W. Cochran, F. S. Bates and D. C. Morse, Design of ABC Block Copolymers Near the ODT with the Random Phase Approximation, *Macromolecules*, 2003, 782–792.
39 L. Zhu, S. Z. D. Cheng, B. H. Calhoun, Q. Ge, R. P. Quirk, E. L. Thomas, B. S. Hsiao, F. Yeh and B. Lotz, Phase Structures and Morphologies Determined by Self-Organization, Vitrification, and Crystallization: Confined Crystallization in an Ordered Lamellar Phase of PEO-B-PS Diblock Copolymer, *Polymer*, 2001, **42**(13), 5829–5839.
40 Y. Ren, T. P. Lodge and M. A. Hillmyer, Effect of Selective Perfluoroalkylation on the Segregation Strength of Polystyrene-1, 2-Polybutadiene Block Copolymers, *Macromolecules*, 2002, **35**, 3889–3894.
41 S. Zhu, W. F. Edmonds, M. A. Hillmyer and T. P. Lodge, Synthesis and Self-Assembly of Highly Incompatible Polybutadiene-Poly(hexafluoropropylene Oxide) Diblock Copolymers, *J. Polym. Sci., Part B: Polym. Phys.*, 2005, **43**(24), 3685–3694.
42 M. A. Hillmyer and T. P. Lodge, Synthesis and Self-Assembly of Fluorinated Block Copolymers, *J. Polym. Sci., Part A: Polym. Chem.*, 2002, **40**(1), 1–8.
43 D. H. C. Wong, A. Vitale, D. Devaux, A. Taylor, A. A. Pandya, D. T. Hallinan, J. L. Thelen, S. J. Mecham, S. F. Lux, A. M. Lapides, P. R. Resnick, T. J. Meyer, R. M. Kostecki, N. P. Balsara and J. M. DeSimone, Phase Behavior and Electrochemical Characterization of Blends of Perfluoropolyether, Poly(ethylene Glycol), and a Lithium Salt, *Chem. Mater.*, 2015, **27**(2), 597–603.
44 W. W. Maurer, F. S. Bates, T. P. Lodge, K. Almdal, K. Mortensen and G. H. Fredrickson, Can a Single Function for χ Account for Block Copolymer and Homopolymer Blend Phase Behavior?, *J. Chem. Phys.*, 1998, **108**(7), 2989–3000.
45 N. P. Balsara, A. A. Lefebvre, J. H. Lee, C. C. Lin and B. Hammouda, Search for a Model Polymer Blend, *AIChE J.*, 1998, **44**(11), 2515–2519.
46 J. Sun, A. A. Teran, X. Liao, N. P. Balsara and R. N. Zuckermann, Nanoscale Phase Separation in Sequence-Defined Peptoid Diblock Copolymers, *J. Am. Chem. Soc.*, 2013, **135**, 14119–14124.
47 S. Lee, T. M. Gillard and F. S. Bates, Fluctuations, Order, and Disorder in Short Diblock Copolymers, *AIChE J.*, 2013, **59**(9), 3502–3513.
48 B. Van Genabeek, B. F. M. De Waal, M. M. J. Gosens, L. M. Pitet, A. R. A. Palmans and E. W. Meijer, Synthesis and Self-Assembly of Discrete Dimethylsiloxane-Lactic Acid Diblock Co-Oligomers: The Dononacontamer and Its Shorter Homologues, *J. Am. Chem. Soc.*, 2016, **138**(12), 4210–4218.
49 H. Takagi, K. Yamamoto, S. Okamoto and S. Sakurai, A Study on the Phase Behavior of Poly(ε-Caprolactone)-Poly(butadiene) Diblock Copolymers: The Influence of Relatively Low-Molecular-Weight Block Copolymers on the Order-Disorder Transition Behavior, *Polymer*, 2015, **67**, 20–27.
50 S. C. Schmidt and M. A. Hillmyer, Morphological Behavior of Model Poly(ethylene-Alt-Propylene)-B-Polylactide Diblock Copolymers, *J. Polym. Sci., Part B: Polym. Phys.*, 2002, **40**(20), 2364–2376.
51 K. Mori, A. Okawara and H. Takeji, Order-Disorder Transition of Polystyrene-Block-Polyisoprene. I. Thermal Concentration Fluctuations in Single-Phase Melts and Solutions and Determination of χ as a Function of Molecular Weight and Composition, *J. Chem. Phys.*, 1996, **104**(19), 7765.

